

Ada3Drift: Adaptive Training-Time Drifting for One-Step 3D Visuomotor Robotic Manipulation

Chongyang Xu^{1*}, Yixian Zou^{2*}, Ziliang Feng¹,
Fanman Meng², and Shuaicheng Liu^{2**}

¹ College of Computer Science, Sichuan University, Chengdu, China

² School of Information and Communication Engineering, University of Electronic Science and Technology of China, Chengdu, China

Abstract. Diffusion-based visuomotor policies effectively capture multimodal action distributions through iterative denoising, but their high inference latency limits real-time robotic control. Recent flow matching and consistency-based methods achieve single-step generation, yet sacrifice the ability to preserve distinct action modes, collapsing multimodal behaviors into averaged, often physically infeasible trajectories. We observe that the compute budget asymmetry in robotics (offline training vs. real-time inference) naturally motivates recovering this multimodal fidelity by shifting iterative refinement from inference time to training time. Building on this insight, we propose Ada3Drift, which learns a training-time drifting field that attracts predicted actions toward expert demonstration modes while repelling them from other generated samples, enabling high-fidelity single-step generation (1 NFE) from 3D point cloud observations. To handle the few-shot robotic regime, Ada3Drift further introduces a sigmoid-scheduled loss transition from coarse distribution learning to mode-sharpening refinement, and multi-scale field aggregation that captures action modes at varying spatial granularities. Experiments on three simulation benchmarks (Adroit, Meta-World, and RoboTwin) and real-world robotic manipulation tasks demonstrate that Ada3Drift achieves state-of-the-art performance while requiring $10\times$ fewer function evaluations than diffusion-based alternatives.

Keywords: Visuomotor Policy Learning · One-Step Generation · 3D Point Cloud · Robotic Manipulation

1 Introduction

Learning visuomotor policies from expert demonstrations has achieved remarkable progress [1, 3, 7, 9, 15, 41]. A central challenge is handling the *multimodal* nature of human demonstrations: for a given observation, multiple valid action strategies may exist. Diffusion Policy [5] and its 3D extension DP3 [37] addressed this challenge through iterative denoising, which progressively refines noisy predictions and naturally preserves distinct action modes. This capability has driven

* Equal contribution

** Corresponding author: liushuaicheng@uestc.edu.cn

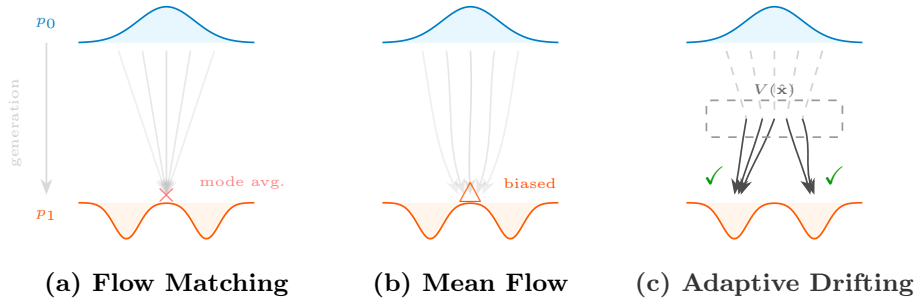


Fig. 1: Single-step generation under multimodal action distributions. (a) Flow Matching: straight conditional paths collapse distinct modes into a single mode average, producing unsafe averaged actions. (b) Mean Flow: adaptive weighting adjusts paths but still converges to a biased mean between modes. (c) Adaptive Drifting (Ours): the drifting field $V(\mathbf{x})$ steers predictions toward true demonstration modes during training via attraction and repulsion, enabling accurate multimodal recovery with 1 NFE at inference.

a wave of diffusion-based robotic systems [2, 18, 20, 23, 32], yet the underlying multi-step denoising process requires 10–100 function evaluations (NFE) per action chunk, creating a fundamental tension with the 10–50 Hz control frequencies demanded by real-time robotic manipulation.

Recent one-step generation methods based on flow matching [14, 28, 39], consistency distillation [19, 25], and diffusion distillation [16, 35] resolve the latency bottleneck by collapsing the generation process into a single forward pass. Yet this speedup comes at a cost: without iterative refinement, their regression-based objectives converge to the *conditional expectation* of target fields [10], averaging over distinct action modes rather than preserving them. In image generation [8], such averaging produces blurry but recognizable outputs. In robotic manipulation, by contrast, the averaged trajectory of two valid strategies (*e.g.*, reaching left vs. right around an obstacle) may drive the gripper straight into the obstacle (Fig. 1). This qualitative difference elevates mode averaging from a quality issue to a *safety concern* in embodied systems.

We observe that robotic systems possess a structural property that enables recovering multimodal fidelity without sacrificing single-step efficiency: **compute budget asymmetry**. Training is performed offline with no latency constraints, while inference must satisfy strict real-time requirements. Current one-step methods discard iterative refinement altogether. We propose instead to *relocate* it: perform all mode-preserving refinement during training, and deploy a single-step generator at inference. The second challenge is **adaptivity**. Unlike large-scale image generation where a fixed recipe succeeds across millions of samples, the few-shot and multi-task nature of robotic learning demands mechanisms that adjust to varying conditions: the number of demonstrations per task is small (typically 10–50), and the geometry of action distributions varies drastically across tasks.

We address both challenges in **Ada3Drift** (**Adaptive 3D Training-Time Drifting**). Ada3Drift employs a training-time drifting field that steers the model’s output distribution toward demonstration modes, while tailoring the mechanism to the robotic regime through sigmoid-scheduled loss transition for few-shot learning, multi-temperature field aggregation for variable action geometries, and a timestep-free architecture enabled by the removal of inference-time iteration.

We summarize our contributions as follows:

- We analyze the mode-averaging problem that arises when accelerating diffusion-based policies to single-step generation, and show that it is qualitatively more severe in robotic action spaces than in image generation. We propose to recover multimodal fidelity by relocating iterative refinement to training time, guided by the compute budget asymmetry of robotic systems.
- We propose Ada3Drift, which realizes this paradigm with designs tailored to the few-shot robotic regime, including sigmoid-scheduled training, multi-scale drifting field aggregation, and a simplified timestep-free architecture.
- Extensive experiments on Adroit [27], Meta-World [21], RoboTwin [22], and real-world manipulation tasks show that Ada3Drift achieves state-of-the-art performance with only 1 NFE, matching or exceeding methods that require 10× more inference compute.

2 Related Work

2.1 Visuomotor Policy Learning

Learning robotic manipulation policies from visual observations has evolved rapidly. Early behavior cloning approaches learn direct mappings from images to actions [9, 15], while recent transformer-based architectures scale to diverse tasks via language conditioning [3, 41] or multi-task pretraining [2, 23, 33]. Action representation has similarly progressed: explicit regression [40] struggles with multimodal demonstrations, motivating energy-based [9] and generative formulations [5]. The choice of visual representation significantly impacts spatial reasoning capability. While 2D image-based policies [3, 5] suffice for planar tasks, they suffer from depth ambiguity and occlusion in 3D manipulation. This has driven a shift toward explicit 3D representations: voxel grids [29], neural feature fields [11, 36], and point clouds [12, 37]. Among these, point clouds offer a favorable balance of geometric fidelity, computational efficiency, and compatibility with downstream policy architectures. Our work builds on this 3D point cloud paradigm, focusing on the orthogonal challenge of preserving multimodal fidelity under single-step generation.

2.2 Diffusion Models in Robotics

Diffusion models [13] have become a dominant paradigm for representing multimodal action distributions in robot learning. Diffusion Policy [5] formulated

policy learning as a conditional denoising process that naturally captures multimodal demonstration strategies. This formulation has been extended along multiple axes: DP3 [37] introduced 3D point cloud conditioning, achieving strong results on Meta-World [21] and Adroit [27]; hierarchical variants [20] decompose long-horizon tasks into sub-goal diffusion; foundation models such as Octo [23] and RDT-1B [18] scale diffusion policies to hundreds of thousands of trajectories; and motion planning methods [4] apply diffusion to trajectory optimization. Despite their expressiveness, all these methods rely on iterative denoising, typically requiring 10–100 NFE. Accelerated samplers such as DDIM [30] reduce but do not eliminate this cost, leaving a computational bottleneck for real-time, high-frequency robotic control.

2.3 Efficient One-Step Policy Generation

Recent research has leveraged Flow Matching (FM) [17] and Consistency Models [25] to mitigate the inference latency of diffusion models. In robotics, approaches like AdaFlow [14], FlowPolicy [39], and MP1 [28] have adapted these techniques to enable efficient 1-step action generation. However, these methods inherit the mode-averaging problem from their underlying regression objectives: the learned generator converges to the conditional expectation [10], producing averaged actions that can be physically infeasible in multimodal scenarios, prompting recent efforts to mitigate this via auxiliary regularizations [31, 42, 43], reinforcement learning [34, 43], or complex architectural additions [38].

Concurrently, Deng *et al.* [6] proposed training-time drifting for image generation, where a drifting field iteratively adjusts the output distribution during training rather than inference. We observe that training-time refinement is *particularly well-suited* to robotic control, where the compute budget asymmetry between offline training and real-time inference is most pronounced and mode averaging carries direct safety implications. However, directly transferring this mechanism to robotics is insufficient: the few-shot data regime, the variable geometry of action distributions across tasks, and the single-step inference requirement all demand adaptive designs. We bridge this gap with adaptive scheduling, multi-scale aggregation, and a streamlined architecture.

3 Method

We present **Ada3Drift**, a single-step 3D visuomotor policy that shifts all iterative refinement from inference time to training time, with designs tailored to the few-shot, multi-task nature of robotic learning. We first formalize the mode-averaging problem in robotic action spaces (Sec. 3.1), then present our training-time refinement framework (Sec. 3.2), and detail the architecture (Sec. 3.3).

3.1 The Speed-Fidelity Trade-off in Policy Generation

Diffusion-based policies [5, 37] effectively preserve multimodal action distributions through iterative denoising: the multi-step refinement process naturally

separates distinct action modes, producing high-fidelity trajectories. However, this quality comes at the cost of 10–100 function evaluations (NFE) per action, far exceeding the latency budget of real-time robotic control at 10–50 Hz.

Flow Matching (FM) [17] offers a path to single-step generation. Given noise $\mathbf{z} \sim p_0$ and target trajectory $\mathbf{a} \sim p_1$, the conditional flow is:

$$\psi_t(\mathbf{z}|\mathbf{a}) = (1-t)\mathbf{z} + t\mathbf{a}, \quad t \in [0, 1], \quad (1)$$

with conditional vector field $u_t(\mathbf{x}|\mathbf{a}) = \mathbf{a} - \mathbf{z}$. A network v_θ regresses this field:

$$\mathcal{L}_{\text{FM}} = \mathbb{E}_{t, \mathbf{z}, \mathbf{a}} [\|v_\theta(\psi_t(\mathbf{z}|\mathbf{a}), t) - (\mathbf{a} - \mathbf{z})\|^2]. \quad (2)$$

While multi-step ODE solvers can still recover multimodal structure, reducing to 1 NFE eliminates this corrective mechanism. The regression objective then drives v_θ toward the *conditional expectation* of target fields, averaging over distinct modes rather than preserving them.

Why mode averaging is catastrophic in action space. In image generation, mode averaging produces blurry but recognizable outputs. In robotic action space, the consequences are qualitatively different and far more severe. Consider a pick-and-place task where the gripper can approach an object from the left or the right. These two strategies define distinct, well-separated modes. Their average is a trajectory that drives the gripper *straight into* the object, producing a collision rather than a grasp. More generally, mode-averaged actions in multimodal scenarios tend to be not merely suboptimal but *physically infeasible* [5]. The challenge, therefore, is to recover the multimodal fidelity that diffusion policies achieve through iterative refinement, while retaining the single-step efficiency of flow-based methods.

3.2 Training-Time Refinement via Drifting Fields

From compute asymmetry to training-time drifting. Robotic systems exhibit a natural asymmetry: training is performed offline on powerful GPUs with no latency constraints, while inference must meet strict real-time requirements. Existing approaches allocate their refinement budget at the wrong time. Diffusion policies [5, 37] spend 10–100 iterative steps at inference, when compute is most scarce. We propose to *invert this allocation*: perform all iterative refinement during training, and generate actions in a single forward at inference.

We achieve this through a **drifting field** that explicitly steers the model’s output distribution toward the modes of expert demonstrations during training. At each training step, the learned drifting field computes per-sample, fine-grained displacement vectors that gently attract generated actions toward their nearest demonstrated strategies while strongly repelling them from other generated samples to maintain rich mode diversity.

However, applying a fixed drifting mechanism to robotic policy learning is insufficient. The few-shot data regime (10–50 demonstrations), the diverse task geometries, and the single-step inference setting each introduce challenges absent in large-scale image generation. We address these through three targeted designs.

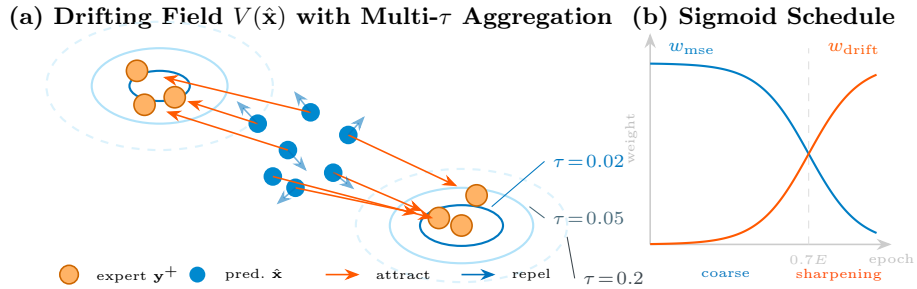


Fig. 2: Mechanism of adaptive drifting. (a) Predictions $\hat{\mathbf{x}}$ are attracted toward expert modes \mathbf{y}^+ and repelled from each other via bidirectional affinity. Concentric contours show multi-temperature field aggregation ($\tau \in \{0.02, 0.05, 0.2\}$): small τ captures tight clusters, large τ covers broader structure. (b) Sigmoid-scheduled loss transitions from MSE-dominated coarse learning to drift-based mode sharpening at $0.7E$.

Drifting field computation. Given a batch of model predictions $\{\mathbf{x}_i\}_{i=1}^N$ and expert demonstrations $\{\mathbf{y}_j^+\}_{j=1}^M$, we compute a soft assignment that matches each prediction to its nearest mode through a bidirectional affinity:

$$A_{ij} = \sqrt{A_{ij}^{\text{row}} \cdot A_{ij}^{\text{col}}}, \quad (3)$$

where A^{row} and A^{col} are row-wise and column-wise softmax normalizations of pairwise distance logits:

$$A_{ij}^{\text{row}} = \frac{\exp(-\|\mathbf{x}_i - \mathbf{y}_j\|/\tau)}{\sum_k \exp(-\|\mathbf{x}_i - \mathbf{y}_k\|/\tau)}, \quad A_{ij}^{\text{col}} = \frac{\exp(-\|\mathbf{x}_i - \mathbf{y}_j\|/\tau)}{\sum_k \exp(-\|\mathbf{x}_k - \mathbf{y}_j\|/\tau)}. \quad (4)$$

The bidirectional normalization ensures balanced assignment: row normalization prevents any prediction from ignoring distant modes, while column normalization prevents popular modes from monopolizing all predictions, as illustrated in Fig. 2 (a). The drifting field for each prediction \mathbf{x}_i is:

$$V(\mathbf{x}_i) = \underbrace{\sum_j W_{ij}^+ \mathbf{y}_j^+}_{\text{attract to real modes}} - \underbrace{\sum_k W_{ik}^- \mathbf{x}_k}_{\text{repel from generated samples}}, \quad (5)$$

where W^+ and W^- are derived from the affinity matrix with cross-set normalization [6]. The attraction term pulls each prediction toward its assigned demonstration mode, while the repulsion term pushes predictions apart to ensure coverage of all modes.

Multi-scale field aggregation. The geometry of action distributions varies drastically across robotic tasks. Grasping tasks may exhibit tightly clustered modes where approach angles differ by millimeters, while bi-manual coordination tasks have widely separated modes corresponding to fundamentally different arm

configurations. A fixed temperature τ captures structure at only one spatial scale, making it unsuitable for a multi-task framework.

To handle this variation, we aggregate drifting fields over multiple temperatures $\{\tau_l\} = \{0.02, 0.05, 0.2\}$:

$$V_{\text{total}}(\mathbf{x}) = \sum_l \frac{V_{\tau_l}(\mathbf{x})}{\lambda_{\tau_l}}, \quad (6)$$

where $\lambda_{\tau_l} = \sqrt{\mathbb{E}[\|V_{\tau_l}\|^2/D]}$ normalizes each field to unit variance, automatically balancing contributions across scales without per-task tuning. Prior to the computation, all samples are normalized such that the average pairwise distance is proportional to \sqrt{D} , where D is the flattened action dimension. This self-normalizing design ensures that the same temperature set works across tasks with vastly different action magnitudes.

Sigmoid-scheduled loss transition. In large-scale image generation with millions of training samples, the drifting field provides useful gradients from the start because the model quickly forms a reasonable output distribution. The few-shot robotics regime presents a fundamentally different challenge: with only 10–50 demonstrations, the model’s initial predictions are too far from any data mode for the soft assignment to produce meaningful drifting vectors.

We address this through a two-phase schedule (Fig.2 (b)) that automatically transitions between learning objectives:

$$\mathcal{L} = w_{\text{drift}}(e) \cdot \mathcal{L}_{\text{drift}} + w_{\text{mse}}(e) \cdot \|\mathbf{x} - \mathbf{y}^+\|^2, \quad (7)$$

where the drift loss $\mathcal{L}_{\text{drift}} = \|\hat{\mathbf{x}} - \text{sg}(\hat{\mathbf{x}} + V_{\text{total}})\|^2$ uses stop-gradient $\text{sg}(\cdot)$ to treat the drifting target as fixed. The weights evolve via sigmoid scheduling:

$$w_{\text{drift}}(e) = \sigma\left(\frac{e - e_{\text{mid}}}{k \cdot E}\right), \quad w_{\text{mse}}(e) = 1 - w_{\text{drift}}(e), \quad (8)$$

with crossover point $e_{\text{mid}} = 0.7E$ and sharpness $k = 0.05$. In the early phase ($e \ll e_{\text{mid}}$), MSE loss dominates and teaches the model the coarse structure of the action distribution. As training progresses and predictions move closer to data modes, the drifting field gradually takes over to sharpen mode separation. The late crossover at 70% of training reflects a key empirical finding: with only few demonstrations, the model requires the majority of training to establish a coarse distribution before drift-based refinement becomes effective.

3.3 Architecture

Ada3Drift takes the robot’s proprioceptive state \mathbf{s}_t and a 3D point cloud \mathbf{P}_t as input, and outputs a horizon of H future actions $\hat{\mathbf{a}}_{t:t+H}$ in a single forward pass. The architecture comprises a 3D observation encoder, a timestep-free action generator, and a receding-horizon execution scheme, as illustrated in Fig.3.

3D Observation Encoder. We encode point cloud observations following the DP3 pipeline [37]. Raw point clouds are first downsampled via Farthest Point

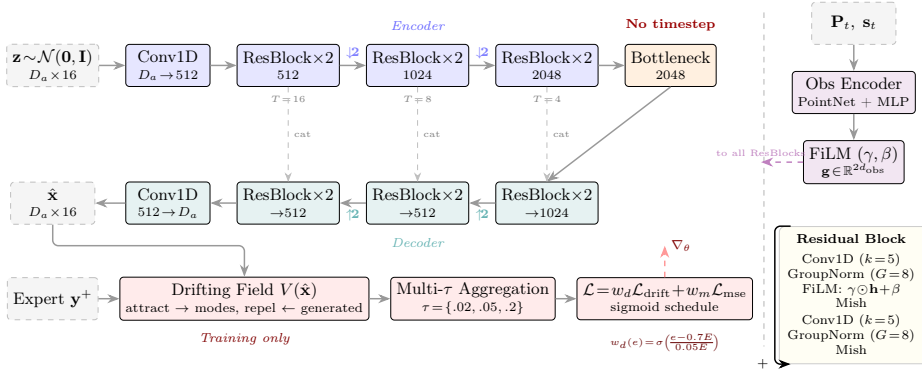


Fig. 3: Overview of Ada3Drift. *Left:* the timestep-free 1D U-Net maps Gaussian noise \mathbf{z} to action trajectories $\hat{\mathbf{x}}$. The encoder (blue) downsamples the temporal dimension; the decoder (teal) upsamples with skip connections. The bottom row (training only) shows the drifting field loss: displacement vectors aggregated across multiple temperatures and combined with MSE loss via sigmoid scheduling. *Right:* the 3D observation encoder extracts a global conditioning vector \mathbf{g} , which modulates every residual block via FiLM. At inference, only the U-Net forward pass is executed (1 NFE).

Sampling (FPS) to a fixed size N_p (512 for Adroit, 1024 for Meta-World and RoboTwin). A PointNet backbone [26] processes 3D coordinates through shared MLPs with channel dimensions [64, 128, 256, 512], followed by max-pooling and a linear projection with LayerNorm, yielding a per-step feature $\mathbf{c}_t \in \mathbb{R}^{d_{\text{obs}}}$ with $d_{\text{obs}} = 64$. The robot’s proprioceptive state \mathbf{s}_t (joint angles, end-effector pose, and gripper state) is separately encoded and concatenated with \mathbf{c}_t before projection. For a temporal observation window of $T_o = 2$ steps, the per-step features are concatenated into a global conditioning vector $\mathbf{g} = [\mathbf{c}_1; \mathbf{c}_2] \in \mathbb{R}^{2d_{\text{obs}}}$.

Timestep-Free Action Generator. In diffusion and flow-based policies, the network is conditioned on a noise level or timestep t via a sinusoidal embedding, because the same architecture must operate across all noise scales during denoising. Since Ada3Drift relocates all refinement to training and generates actions in a single pass, this conditioning is unnecessary. We remove the timestep embedding and its projection layers entirely, yielding a simpler architecture.

The generator is a 1D convolutional U-Net that directly maps Gaussian noise $\mathbf{z} \in \mathbb{R}^{D_a \times H}$ to an action trajectory, where D_a is the action dimension and $H = 16$ is the prediction horizon. The network is organized symmetrically across three resolution levels with channel dimensions [512, 1024, 2048]. The *encoder path* contains three stages, each with two residual blocks and a strided downsampling convolution that halves the temporal resolution ($H \rightarrow H/2 \rightarrow H/4$). Two residual blocks at the coarsest resolution form the *bottleneck*. The *decoder path* mirrors the encoder with nearest-neighbor upsampling; each decoder stage receives skip connections from its corresponding encoder stage via channel concatenation, then reduces back to the target dimension through two residual blocks.

Each residual block contains two Conv1D layers (kernel size 5, padding 2) with GroupNorm ($G = 8$ groups) and Mish activations, plus a residual shortcut (1×1 convolution when channel dimensions differ, identity otherwise). The observation features modulate intermediate representations via FiLM conditioning [24] applied at *every* residual block:

$$\mathbf{h}' = \gamma(\mathbf{g}) \odot \text{GroupNorm}(\text{Conv}(\mathbf{h})) + \beta(\mathbf{g}), \quad (9)$$

where $\gamma, \beta \in \mathbb{R}^C$ are per-channel scale and bias vectors predicted from \mathbf{g} through a Mish-activated linear layer. This pervasive conditioning ensures that action generation is tightly coupled to the observation context at all spatial scales. A final Conv1D block followed by a 1×1 convolution projects the decoder output back to the action dimension D_a .

Receding-Horizon Execution. At test time, action generation requires exactly one forward pass: sample $\mathbf{z} \sim \mathcal{N}(\mathbf{0}, \mathbf{I})$, compute $\hat{\mathbf{a}} = f_\theta(\mathbf{z}, \mathbf{g})$, and extract the executable chunk $\hat{\mathbf{a}}_{T_o-1:T_o-1+N_a}$ with execution length $N_a = 8$ from the full $H = 16$ horizon. This receding-horizon scheme allows the policy to correct for prediction drift by re-planning every N_a steps. The entire pipeline yields **1 NFE** per action chunk, compared to 10–100 NFE for diffusion-based policies, enabling real-time control at the frequencies required by physical robotic systems.

4 Experiments

We evaluate Ada3Drift on simulation benchmarks of increasing complexity and real-world robotic manipulation tasks.

4.1 Experimental Setup

Benchmarks. Following FlowPolicy [39], we first evaluate on **Adroit** [27] (3 dexterous manipulation tasks with a 24-DoF Shadow Hand) and **Meta-World** [21] (34 tasks on a Sawyer arm, grouped into Easy (21), Medium (4), Hard (4), and Very Hard (5)) with 10 expert demonstrations per task. To further assess 3D perception capability, we select 8 representative tasks from the **RoboTwin** [22] simulation platform on the Agilx Cobot Magic robot, each requiring precise spatial reasoning from point cloud observations. Finally, following the real-world evaluation protocol of MP1 [28], we design 5 manipulation tasks on a physical Agilx Cobot Magic robot inspired by RoboTwin task designs, each trained from 20 expert demonstrations and evaluated over 20 trials.

Baselines. We compare against two categories of methods: (i) *Image-based*: Diffusion Policy (DP) [5], AdaFlow [14], and Consistency Policy (CP) [25], with results cited from [39]; (ii) *3D point cloud-based*: DP3 [37], Simple DP3 [37], FlowPolicy [39], and MP1 [28], all reproduced under identical settings. Among these, DP, DP3, and Simple DP3 use iterative generation (10 NFE), while CP, FlowPolicy, MP1, and Ada3Drift achieve single-step generation (1 NFE).

Implementation Details. We use a compact observation consisting of the robot’s proprioceptive state and a 3D point cloud, downsampled via FPS to

Table 1: Comparison on Adroit [27] and Meta-World [21] with 10 expert demonstrations. We evaluate against **image-based** (*, cited from [39]) and **3D point cloud-based** baselines (reproduced). Best 3D results in **bold**.

Methods	NFE	Adroit			Meta-World				Avg.
		Hammer	Door	Pen	Easy	Medium	Hard	V. Hard	
DP* [5]	10	16±10	34±11	13±2	50.7±6.1	11.0±2.5	5.3±2.5	22.0±5.0	35.2±5.3
AdaFlow* [14]	–	45±11	27±6	18±6	49.4±6.8	12.0±5.0	5.8±4.0	24.0±4.8	35.6±6.1
CP* [25]	1	45±4	31±10	13±6	69.3±4.2	21.2±6.0	17.5±3.9	30.0±4.9	50.1±4.7
DP3 [37]	10	88.7±1.2	64.2±6.5	59.7±3.1	85.5±1.9	64.0±3.5	58.6±1.4	71.5±2.5	78.0±2.4
Simple DP3 [37]	10	86.0±2.4	61.0±4.5	61.0±2.8	85.9±1.9	64.3±3.7	61.1±3.4	70.7±2.5	78.3±2.7
FlowPolicy [39]	1	77.0±2.2	61.2±4.7	58.0±4.1	84.3±2.6	62.7±3.2	61.1±3.5	71.2±2.7	77.0±3.0
MP1 [28]	1	84.3±3.1	64.2±3.5	57.7±4.5	85.8±1.5	62.2±7.5	62.3 ±2.0	74.4±4.3	78.6±3.2
Ada3Drift	1	90.3 ±0.9	65.0 ±3.6	63.3 ±3.1	86.7 ±1.7	62.3 ±2.7	60.7±6.2	72.7 ±4.5	79.2 ±2.8

* Results are cited from FlowPolicy [39]. All other baselines are reproduced on a single RTX 4090D.

Table 2: Comparison on RoboTwin [22] single-arm tasks. All methods use 3D point cloud input. Best results in **bold**.

Methods	NFE	Beat Block	Click Alarm	Open Microwave	Place Cup	Place Phone	Stack Blocks	Stack Bowls	Turn Switch	Avg.
DP3 [37]	10	63.7 ±2.6	83.0 ±2.2	95.0 ±2.2	58.7 ±5.4	43.7 ±8.2	30.0 ±1.6	82.0 ±6.2	44.3 ±4.5	62.5
FlowPolicy [39]	1	56.3 ±1.2	97.0 ±0.0	66.3 ±3.7	76.7 ±1.2	55.5 ±5.5	10.7 ±2.4	61.7 ±1.7	42.7 ±2.1	58.4
MP1 [28]	1	79.0 ±1.6	95.0 ±1.4	94.7 ±1.2	81.0 ±3.7	41.0 ±2.2	23.7 ±1.2	86.3 ±2.1	46.0 ±1.4	68.3
Ada3Drift	1	81.3 ±3.4	97.7 ±1.2	97.7 ±1.2	86.7 ±0.5	46.7 ±5.4	21.0 ±2.8	88.3 ±1.7	50.0 ±4.3	71.2

512 points (Adroit) or 1024 points (Meta-World, RoboTwin). The observation horizon is 2 steps. We use 10 expert demonstrations per task for Adroit and Meta-World. All models are trained on a single NVIDIA RTX 4090D with AdamW ($\text{lr} = 10^{-4}$, batch size 128). We report success rates averaged over 3 seeds, evaluating checkpoints every 200 epochs and reporting the mean of the top-5 checkpoints per seed.

4.2 Main Results

Adroit and Meta-World. Tab. 1 presents the comparison on Adroit and Meta-World. Among 1-step methods, Ada3Drift achieves the highest average success rate (78.9%), outperforming both FlowPolicy (77.0%) and MP1 (78.6%). Notably, Ada3Drift surpasses MP1 on 5 out of 7 task categories, with particularly strong gains on Adroit Hammer (+6.0%), Pen (+5.6%), and Meta-World Easy (+0.9%). Ada3Drift also matches or exceeds the multi-step DP3 baseline (78.0%, 10 NFE) with 10× fewer function evaluations, demonstrating that training-time refinement can fully compensate for the loss of inference-time iteration. The one category where Ada3Drift underperforms MP1 is Meta-World Hard (58.7% vs. 62.3%). We attribute this to the high action-space variance of hard tasks, where the sigmoid schedule may benefit from task-specific tuning of the crossover point.

Table 3: Ablation study. We progressively add components to the DP3 backbone. Top-5 checkpoint mean over 3 seeds; categories follow Tab. 1.

Variant	NFE	Adroit			Meta-World				Avg.
		Ham.	Door	Pen	Easy	Med.	Hard	V.Hard	
DP3 [37]	10	88.7	64.2	59.7	85.5	64.0	58.6	71.5	78.0
Naive Drifting	1	85.7	61.7	54.8	81.8	69.5	66.7	61.8	75.0
Ada3Drift	1	90.3	65.0	63.3	86.7	62.3	58.7	72.7	78.9

RoboTwin. Tab. 2 evaluates all methods on 8 manipulation tasks from the RoboTwin benchmark, which requires precise spatial reasoning from point cloud observations. Ada3Drift achieves the highest average success rate of 71.2%, significantly outperforming DP3, FlowPolicy, and MP1. Ada3Drift ranks first on 6 out of 8 tasks, with particularly large margins on Place Cup (86.7% vs. 81.0% for MP1, +5.7%), Turn Switch (50.0% vs. 46.0%, +4.0%), and Open Microwave (97.7% vs. 94.7%, +3.0%). Notably, Ada3Drift surpasses the multi-step DP3 by 8.7% on average despite using only a single forward pass, highlighting the advantage of explicit mode separation over iterative refinement in tasks with complex 3D contact geometry. FlowPolicy struggles on tasks that require extended sequential reasoning such as Open Microwave (66.3%) and Stack Bowls (61.7%), where mode-averaged trajectories fail to maintain consistent contact.

4.3 Analysis and Ablation

Component ablation. Tab. 3 isolates the contribution of each design choice. Starting from the DP3 backbone (10 NFE), we first replace the iterative DDIM sampler with a single-step drifting generator. This Naive Drifting variant degrades the overall success rate by 3.0% (75.0% vs. 78.0%), with the most notable drops on Adroit Pen (−4.9%) and Meta-World Very Hard (−9.7%). The degradation is expected: without curriculum control, the drifting loss dominates early training and destabilizes the base reconstruction objective before the network has learned meaningful action representations. Adding adaptive drift, *i.e.*, multi-temperature aggregation ($\tau \in \{0.02, 0.05, 0.2\}$) combined with sigmoid loss scheduling, yields our full Ada3Drift model. This not only recovers but surpasses DP3 (78.9% vs. 78.0%) in a single forward pass, achieving a 10× reduction in inference cost. The improvement over Naive Drifting is consistent across all Adroit tasks, with the largest gain on Pen (+8.5%) and Hammer (+4.6%). These results validate that both components of adaptive drift are essential: multi-scale temperature aggregation captures mode structures at different granularities, while the sigmoid schedule delays drift optimization until the base policy has stabilized, preventing destructive interference in early training.

Inference speed. Tab. 4 compares inference throughput on the Adroit Door task (single RTX 4090D, batch size 1). DP3 requires 10 sequential DDIM steps and runs at only 18.7 Hz,

Table 4: Inference speed. Single RTX 4090D, batch 1.

Method	NFE	Hz \uparrow	ms \downarrow
DP3	10	18.7	53.4
FlowPolicy	1	274.4	3.6
MP1	1	249.5	4.0
Ada3Drift	1	233.9	4.3

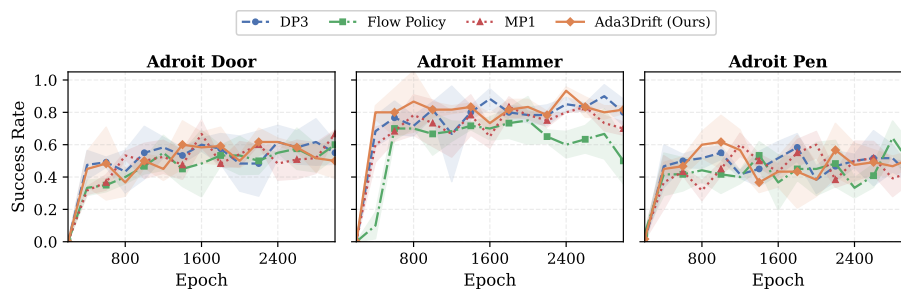


Fig. 4: Training curves on Adroit dexterous manipulation tasks. Success rate (mean \pm std over 3 seeds) versus training epoch. Ada3Drift consistently matches or outperforms other single-step methods (Flow Policy, MP1) across all three tasks.

which is marginal for real-time control. All single-step methods eliminate this bottleneck: FlowPolicy reaches 274.4 Hz, MP1 249.5 Hz, and Ada3Drift 233.9 Hz (4.3 ms per step), representing a $12.5\times$ speedup over DP3. Although Ada3Drift is slightly slower than FlowPolicy and MP1 due to its larger U-Net with temporal attention, all three comfortably exceed the 10 Hz control frequency typical in robotic manipulation, confirming that single-step generation is practical for closed-loop deployment.

Training dynamics. Fig. 4 plots the success rate over training epochs on three Adroit tasks. On Hammer, Ada3Drift establishes a clear lead from epoch 600 and maintains it throughout, reaching a final success rate above 90%. On Door, all single-step methods converge to similar performance, though Ada3Drift shows less variance across seeds. The most informative comparison is on Pen, a highly multimodal task where the Shadow Hand must coordinate 24 joints: here Ada3Drift gradually separates from FlowPolicy and MP1 in the later epochs, consistent with the sigmoid schedule activating the drift loss after the base policy has stabilized. Across all three tasks, Ada3Drift converges at a similar rate to the baselines, confirming that the drifting field improves final performance without slowing down early-stage learning.

Qualitative analysis. Fig. 5 visualizes rollout sequences of FlowPolicy, MP1, and Ada3Drift on two RoboTwin tasks that demand precise 3D positioning: Stack Blocks and Place Phone Stand. In Stack Blocks, FlowPolicy and MP1 produce hesitant grasping motions and imprecise placement, frequently dropping the block beside the target or failing to align the gripper. Ada3Drift, by contrast, executes a clean reach-grasp-place sequence with smooth end-effector trajectories. A similar pattern appears in Place Phone Stand: the baselines exhibit jittery wrist rotations near the placement pose, a hallmark of mode-averaging in multimodal action spaces, whereas Ada3Drift commits to a single coherent mode and completes the task decisively. These qualitative differences are consistent with our drifting field design, which repels predictions away from the inter-mode average and attracts them toward nearby expert modes. The visual improvement translates directly into higher success rates on these precision-critical tasks.

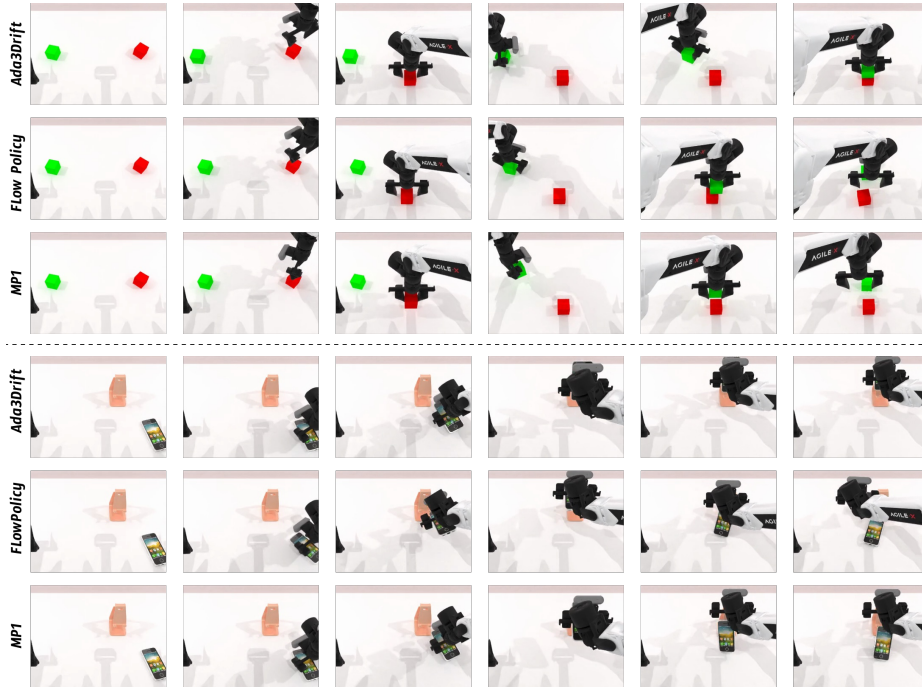


Fig. 5: Qualitative comparison. Predicted action trajectories of FlowPolicy, MP1, and Ada3Drift on representative tasks. Ada3Drift generates trajectories that better align with the expert demonstrations, especially in multimodal scenarios.

4.4 Real-World Experiments

We deploy Ada3Drift on a physical Agilx Cobot Magic robot using a single arm, training each task from 20 teleoperated expert demonstrations and reporting success rates over 20 trials. We evaluate five manipulation tasks: (i) **Cup on Coaster**: place a cup precisely onto a coaster; (ii) **Stack Blocks**: stack two same-color blocks; (iii) **Stack Plates**: stack two plates; (iv) **Close Drawer**: push a drawer closed; (v) **Spoon in Bowl**: place a spoon into a bowl. These tasks span a range of manipulation primitives including precise placement, stacking, and pushing, all requiring accurate 3D spatial reasoning capability from point cloud observations.

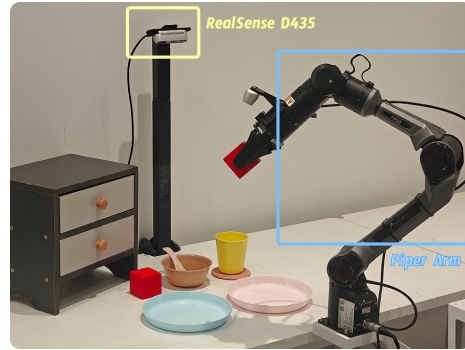


Fig. 6: Real-world task execution. Keyframe sequences of Ada3Drift on the Agilx Cobot Magic robot.

Table 5: Real-world experiments on a physical Agilx Cobot Magic robot. Each task is trained from 20 expert demonstrations and evaluated over 20 trials. Best results in **bold**.

Methods	Cup on Coaster	Stack Blocks	Stack Plates	Close Drawer	Spoon in Bowl	Avg.
DP3 [37]	70	55	60	90	65	68
FlowPolicy [39]	75	25	55	80	50	57
MP1 [28]	75	45	80	85	60	69
Ada3Drift	85	60	90	90	70	79

Real-world analysis. Tab. 5 reports success rates for all methods. Ada3Drift achieves the highest average success rate of 79%, outperforming DP3 (68%), FlowPolicy (57%), and MP1 (69%) by substantial margins. The advantage is most pronounced on tasks requiring precise placement: Stack Blocks (60% vs. 45% for MP1) and Stack Plates (90% vs. 80% for MP1), where mode-averaging baselines struggle to commit to a single stable grasp-and-place strategy. On Cup on Coaster, Ada3Drift reaches 85%, 10% above both FlowPolicy and MP1, confirming that the drifting field’s mode-sharpening effect transfers reliably to real-world settings. FlowPolicy performs notably worse on the physical robot (57% average) than in simulation, suggesting that its mode-averaged trajectories are less robust to real-world perturbations such as sensor noise and calibration errors. Fig. 6 shows representative keyframes of Ada3Drift executing these tasks, demonstrating smooth and decisive manipulation behavior consistent with our simulation findings.

5 Conclusion

We present Ada3Drift, a single-step 3D visuomotor policy that shifts iterative refinement from inference to training. It introduces a drifting field that pulls predicted actions toward expert modes while pushing them away from other generated samples, enabling high-fidelity one-step action generation from 3D point cloud observations. To address the few-shot robotic setting, Ada3Drift incorporates adaptive drift, including a sigmoid-scheduled loss transition to avoid early-stage interference and multi-temperature field aggregation to capture action modes at different spatial scales. Extensive experiments on three simulation benchmarks (Adroit, Meta-World, and RoboTwin) and five real-world manipulation tasks show that Ada3Drift achieves state-of-the-art performance among single-step methods, while matching or surpassing multi-step diffusion baselines that require $10\times$ more function evaluations. On the physical Agilx Cobot Magic robot, it achieves a 79% average success rate, outperforming all baselines. It also produces smoother, more decisive trajectories, avoiding the mode-averaging artifacts of flow matching and mean flow methods.

References

1. Bharadhwaj, H., Mottaghi, R., Gupta, A., Tulsiani, S.: Track2act: Predicting point tracks from internet videos enables generalizable robot manipulation. In: ECCV (2024) [1](#)
2. Black, K., Brown, N., Driess, D., Esmail, A., Equi, M., Finn, C., Fusai, N., Groom, L., Hausman, K., Ichter, B., et al.: π_0 : A vision-language-action flow model for general robot control. In: RSS (2025) [2](#), [3](#)
3. Brohan, A., Brown, N., Carbajal, J., et al.: Rt-1: Robotics transformer for real-world control at scale. In: arXiv preprint arXiv:2212.06817 (2022) [1](#), [3](#)
4. Carvalho, J.A., Le, A.T., Baierl, M., Koert, D., Peters, J.: Motion policy networks. In: CoRL. pp. 1654–1663 (2023) [4](#)
5. Chi, C., Feng, S., Du, Y., Xu, Z., Cousineau, E., Burchfiel, B., Song, S.: Diffusion policy: Visuomotor policy learning via action diffusion. In: RSS (2023) [1](#), [3](#), [4](#), [5](#), [9](#), [10](#)
6. Deng, M., Li, H., Li, T., Du, Y., He, K.: Generative modeling via drifting (2026), <https://arxiv.org/abs/2602.04770> [4](#), [6](#)
7. Ding, P., Zhao, H., et al.: Quar-vla: Vision-language-action model for quadruped robots. In: ECCV (2024) [1](#)
8. Esser, P., Kulal, S., Blattmann, A., et al.: Scaling rectified flow transformers for high-resolution image synthesis. In: ICML (2024) [2](#)
9. Florence, P., Lynch, C., Zeng, A., Ramirez, O.A., Wahid, A., Downs, L., Wong, A., Lee, J., Mordatch, I., Tompson, J.: Implicit behavioral cloning. In: CoRL. pp. 158–168 (2022) [1](#), [3](#)
10. Geng, Z., Deng, M., Bai, X., Kolter, J.Z., He, K.: Mean flows for one-step generative modeling. In: NeurIPS (2025) [2](#), [4](#)
11. Gervet, T., Xian, Z., Gkanatsios, N., Fragkiadaki, K.: Act3d: 3d feature field transformers for multi-task robotic manipulation. In: CoRL (2023) [3](#)
12. Goyal, A., Blukis, V., Xu, J., Guo, Y., Chao, Y.W., Fox, D.: Rvt2: Learning precise manipulation from few demonstrations. In: RSS (2024) [3](#)
13. Ho, J., Jain, A., Abbeel, P.: Denoising diffusion probabilistic models. In: NeurIPS. vol. 33, pp. 6840–6851 (2020) [3](#)
14. Hu, X., qiang liu, Liu, X., Liu, B.: Adaflow: Imitation learning with variance-adaptive flow-based policies. In: NeurIPS (2024), <https://openreview.net/forum?id=ugXKInqDCC> [2](#), [4](#), [9](#), [10](#)
15. Jang, E., Irpan, A., Khansari, M., Kappler, D., Ebert, F., Lynch, C., Levine, S., Finn, C.: BC-Z: Zero-shot task generalization with robotic imitation learning. In: CoRL. pp. 991–1002 (2022) [1](#), [3](#)
16. Jia, B., Ding, P., Cui, C., Sun, M., Qian, P., Huang, S., Fan, Z., Wang, D.: Score and distribution matching policy: Advanced accelerated visuomotor policies via matched distillation (2024), <https://arxiv.org/abs/2412.09265> [2](#)
17. Lipman, Y., Chen, R.T.Q., Ben-Hamu, H., Nickel, M., Le, M.: Flow matching for generative modeling. In: ICLR (2023), <https://openreview.net/forum?id=PqvMRDCJT9t> [4](#), [5](#)
18. Liu, S., Wu, L., Li, B., Tan, H., Chen, H., Wang, Z., Xu, K., Su, H., Zhu, J.: RDT-1b: a diffusion foundation model for bimanual manipulation. In: ICLR (2025), <https://openreview.net/forum?id=yAzN4tz7oI> [2](#), [4](#)
19. Lu, G., Yang, Z., Lan, Z., Chen, T., Mu, Y., Xu, M., Peng, S., Yu, Q., Liang, Z.: Manicm: Real-time 3d diffusion policy via consistency model for robotic manipulation. arXiv preprint arXiv:2406.01586 (2024) [2](#)

20. Ma, X., Patidar, S., Haughton, I., James, S.: Hierarchical diffusion policy for kinematics-aware multi-task robotic manipulation. CVPR (2024) [2](#), [4](#)
21. McLean, R., Chatzaroulas, E., McCutcheon, L., Röder, F., Yu, T., He, Z., Zentner, K., Julian, R., Terry, J.K., Woungang, I., Farsad, N., Castro, P.S.: Meta-world+: An improved, standardized, RL benchmark. In: NeurIPS (2025), <https://openreview.net/forum?id=1de3azE606> [3](#), [4](#), [9](#), [10](#)
22. Mu, Y., Chen, T., Chen, Z., Peng, S., Lan, Z., Gao, Z., Liang, Z., Yu, Q., Zou, Y., Xu, M., et al.: Robotwin: Dual-arm robot benchmark with generative digital twins. In: CVPR (2025) [3](#), [9](#), [10](#)
23. Octo Model Team, Ghosh, D., Walke, H., Pertsch, K., Black, K., Mees, O., Dasari, S., Hejna, J., Kreiman, T., Xu, C., et al.: Octo: An open-source generalist robot policy. RSS (2024) [2](#), [3](#), [4](#)
24. Perez, E., Strub, F., De Vries, H., Dumoulin, V., Courville, A.: FiLM: Visual reasoning with a general conditioning layer. In: AAAI. vol. 32 (2018) [9](#)
25. Prasad, A., Lin, K., Wu, J., Zhou, L., Bohg, J.: Consistency policy: Accelerated visuomotor policies via consistency distillation. In: RSS (2024) [2](#), [4](#), [9](#), [10](#)
26. Qi, C.R., Su, H., Mo, K., Guibas, L.J.: Pointnet: Deep learning on point sets for 3d classification and segmentation. In: CVPR. pp. 652–660 (2017) [8](#)
27. Rajeswaran, A., Kumar, V., Gupta, A., Vezzani, G., Schulman, J., Todorov, E., Levine, S.: Learning Complex Dexterous Manipulation with Deep Reinforcement Learning and Demonstrations. In: RSS (2018) [3](#), [4](#), [9](#), [10](#)
28. Sheng, J., Wang, Z., Li, P., Liu, M.: Mp1: Meanflow tames policy learning in 1-step for robotic manipulation. In: AAAI (2026) [2](#), [4](#), [9](#), [10](#), [14](#)
29. Shridhar, M., Manuelli, L., Fox, D.: Perceiver-actor: A multi-task transformer for robotic manipulation. In: CoRL (2022) [3](#)
30. Song, J., Meng, C., Ermon, S.: Denoising diffusion implicit models. In: ICLR (2021) [4](#)
31. Su, Y., Liu, N., Chen, D., Zhao, Z., Wu, K., Li, M., Xu, Z., Che, Z., Tang, J.: Freqpolicy: Efficient flow-based visuomotor policy via frequency consistency. In: NeurIPS (2025), <https://openreview.net/forum?id=NKNryrCGYn> [4](#)
32. Vosylius, V., Johns, E.: Instant policy: In-context imitation learning via graph diffusion. In: ICLR (2025), <https://openreview.net/forum?id=je3GZissZc> [2](#)
33. Wang, L., Chen, X., Zhao, J., He, K.: Scaling proprioceptive-visual learning with heterogeneous pre-trained transformers. In: NeurIPS (2024) [3](#)
34. Wang, Z., Li, D., Chen, Y., Shi, Y., Bai, L., Yu, T., Fu, Y.: One-step generative policies with q-learning: A reformulation of meanflow. In: AAAI (2025), <https://arxiv.org/abs/2511.13035> [4](#)
35. Wang, Z., Hunt, J.J., Zhou, M.: One-step diffusion policy: Fast visuomotor policies via diffusion distillation. In: ICML (2024) [2](#)
36. Ze, Y., Yan, G., Wu, Y.H., Macaluso, A., Ge, Y., Ye, J., Hansen, N., Li, L.E., Wang, X.: GNFactor: Multi-task real robot learning with generalizable neural feature fields. In: CoRL. pp. 284–301 (2023) [3](#)
37. Ze, Y., Zhang, G., Zhang, K., Hu, C., Wang, M., Xu, H.: 3d diffusion policy: Generalizable visuomotor policy learning via simple 3d representations. In: RSS (2024) [1](#), [3](#), [4](#), [5](#), [7](#), [9](#), [10](#), [11](#), [14](#)
38. Zhai, X., Zhao, Q., Yu, Q., Hao, C.: Vfp: Variational flow-matching policy for multi-modal robot manipulation (2025), <https://arxiv.org/abs/2508.01622> [4](#)
39. Zhang, Q., Liu, Z., Fan, H., Liu, G., Zeng, B., Liu, S.: Flowpolicy: Enabling fast and robust 3d flow-based policy via consistency flow matching for robot manipulation. In: AAAI. vol. 39, pp. 14754–14762 (2025) [2](#), [4](#), [9](#), [10](#), [14](#)

40. Zhao, T.Z., Kumar, V., Levine, S., Finn, C.: Learning fine-grained bimanual manipulation with low-cost hardware. In: RSS (2023) 3
41. Zitkovich, B., Yu, T., et al.: Rt-2: Vision-language-action models transfer web knowledge to robotic control. In: CoRL. pp. 2165–2183 (2023) 1, 3
42. Zou, G., Wang, H., Wu, H., Qian, Y., Wang, Y., Li, W.: Dm1: Meanflow with dispersive regularization for 1-step robotic manipulation (2025), <https://arxiv.org/abs/2510.07865> 4
43. Zou, G., Wang, H., Wu, H., Qian, Y., Wang, Y., Li, W.: One step is enough: Dispersive meanflow policy optimization (2026), <https://arxiv.org/abs/2601.20701> 4